Available online at www.sciencedirect.com
ScienceDirect
Journal of Nuclear Materials 367–370 (2007) 286–291
journal of nuclear materials
www.elsevier.com/locate/jnucmat

# Lattice kinetic Monte-Carlo modelling of helium–vacancy cluster formation in bcc iron

V.A. Borodin [a,b,*], P.V. Vladimirov [b], A. Möslang [b]

[a] RRC Kurchatov Institute, Kurchatov Sq., 1, 123182 Moscow, Russia
[b] Forschungszentrum Karlsruhe GmbH, Institut für Materialforschung I, P.O. Box 36 40, 76021 Karlsruhe, Germany

**Abstract**

The decomposition of a uniform solid solution of helium atoms and vacancies in bcc iron at 300 °C is investigated by lattice kinetic Monte-Carlo with binding and mobility parameters for vacancies and helium atoms from recently published *ab initio* calculations. It is demonstrated that He–vacancy binding results in the formation of stable and highly mobile small He–V complexes, which play an essential part in the He clustering kinetics.


*PACS:* 61.72.Yx; 61.80.Az

## 1. Introduction

Ferritic-martensitic steels will accumulate substantial amounts of helium in the radiation environment of fusion reactors, which promotes pronounced helium clustering [1,2].

An efficient approach to simulation of He cluster nucleation and growth in irradiated steel should combine quantum mechanical (*ab initio*) modeling of He–V cluster energies, atomistic kinetic Monte-Carlo (KMC) and longer timescale techniques such as object KMC [3] or rate theory. *Ab initio* energies for vacancies, He atoms and their clusters in bcc iron have been reported only recently [4–8]. Monte-Carlo simulations of He clustering [9] are still rare.

The binding between He atoms and vacancies extends to the second nearest neighbor (NN) separations [4,10], creating favorable conditions for the long-range diffusion of at least a bound vacancy – substitutional He pair via the ring diffusion mechanism [11]. The mobility of other small clusters $He_nV_m$ (with $m > n$) also should not be excluded. Here lattice kinetic Monte-Carlo (LKMC) simulations were used to estimate how the mobility of small He–V clusters and the associated cluster coalescence influence the kinetics of He bubble nucleation in bcc iron.

## 2. Simulation details

Simulations have been performed using CASINO-LKMC code. The cubic simulation cell

* Corresponding author. Address: RRC Kurchatov Institute, Kurchatov Sq., 1, 123182 Moscow, Russia. Tel.: +7 095 1969766; fax: +7 095 8825804.
*E-mail address:* borodin@dni.polyn.kiae.su (V.A. Borodin).

0022-3115/$ - see front matter 
doi:10.1016/j.jnucmat.2007.03.137

with bcc lattice and periodic boundary conditions contained ~4.2 million lattice sites. Helium concentrations varied in the range 10–1000 appm, while the vacancy concentration was 100 ppm. The KMC algorithm is of 'continuous time' kind [12], where each Monte-Carlo step (MCS) represents one successful jump and the time per jump is tracked.

The particle jump frequencies $P$ were calculated as

$$P = v_0 \exp(-(E_{sp} - E_{in})/k_B T),$$

where $v_0$ is an attempt frequency, $E_{sp}$ and $E_{in}$ are the energies in the saddle point and before the jump, respectively, and $k_B T$ has its usual meaning.

The equilibrium energies of atomic configurations are calculated in the framework of 'bond model' approximation, where pair-wise interactions between individual atomic species (including vacancies) are represented by virtual bonds with energies $\varepsilon_{A-B}$ depending only on the chemical nature of species A and B terminating a bond and on the bond length, while the total crystal energy $E$ is approximated as

$$E = \sum_k \sum_{A,B} \varepsilon_{A-B}(k) n_{A-B}(k), \quad (1)$$

where $n_{A-B}(k)$ is the number of available pairs of species A and B terminating bonds corresponding to the $k$th nearest neighbour (NN) distance between atoms in the lattice. $\varepsilon_{A-B}$ can be related to the binding energy (that is – the energy required in order to separate a pair A–B from the $k$th NN separation to infinity), $E^b_{A-B}$, as

$$E^b_{A-B}(k) = \varepsilon_{A-Fe}(k) + \varepsilon_{B-Fe}(k) - \varepsilon_{A-B}(k) - \varepsilon_{Fe-Fe}(k),$$

In turn, the defect binding energies can be determined by first principles simulations. Here the literature *ab initio* data for vacancies [5,6], small vacancy clusters [6,7] and small vacancy–helium clusters [4] in bcc iron were used. Bonds up to the second NN shell were included in calculations. The energy values used are summarized in Table 1; they were fitted to the *ab initio* data using Eq. (1).

The saddle point energy was approximated as $E_{sp} = E_m + \max(E_{in}, E_{fi})$, where $E_{fi}$ is the energy after jump and $E_m$ is the migration barrier, which depends on the kind of atom jumping into the vacancy (see Table 1). The barrier employed for He–vacancy exchange was chosen as a trade-off between *ab initio* predictions and calculation limitations. Indeed, while in LKMC all atoms are located strictly on lattice sites, this is not necessarily true for He in real He–V clusters. For example, in the $HeV_2$ complex the He atom can be located between two vacant sites [4]. In order to adequately reproduce the behavior of such clusters by LKMC, we use such barrier for He–V position exchange, so that a helium atom can visit all vacancies in a cluster many times between consecutive vacancy-iron exchanges.

Table 1
Energy parameters used in calculations

| | 1NN | 2NN |
|---|---|---|
| *Bond energies (eV)*[a] | | |
| V–Fe | 0.26 | 0 |
| He–Fe | 0.53 | 0 |
| V–V | 0.36 | −0.3 |
| V–He | 0.27 | −0.53 |
| He–He | 0.25 | −0.74 |
| *Exchange barriers $E_m$ (eV)* | | |
| V–Fe | 0.67 | |
| V–He | 0.6 | |

[a] With respect to Fe–Fe bond.

Small (2–4 vacancies) vacancy clusters have decreased migration barriers for the 'in-cluster' jumps of constituting vacancies [6], which result in the change of cluster shape and/or center of mass position, but do not break the cluster apart. The whole set of the cluster migration barriers from [6] can be closely (with errors less then 0.05) appoximated assuming that the vacancy diffusion jump barrier is decreased by ~0.16 eV per each vacancy in a ring of six lattice sites nearest to the saddle point of the jump (a so-called jump lens). In order to at least partially reproduce this effect, we decreased the barrier for a host atom jump into a vacancy by 0.16, when the jump lens for the jump contained at least one vacancy. In larger voids and bubbles this leads to the acceleration of surface vacancy diffusion as compared to the bulk.

## 3. Simulation results

In order to estimate the influence of He–vacancy binding on He clustering kinetics, three model systems were considered. First of all, only the binding between He atoms was taken into account, while the vacancies acted solely as He transporting agents. In the second set of simulations, the He–vacancy binding was still neglected, but binding between vacancies was included. Finally, all interactions were considered. All simulation runs were performed at $T = 573$ K.

### 3.1. Vacancy-assisted vs. direct He diffusion

He atoms are strongly bound at both the first and second NN separations [4], so that the natural LKMC annealing outcome in the case of no He–V and V–V interaction was He agglomeration in purely He clusters, while the vacancies remained free in the bulk. Unfortunately, the simulations of He clustering in this way is computationally very inefficient, because only a small fraction of vacancy jumps results in He movement. After 300 millions MCSs (corresponding to ~7 ms of real time) the clustering was still at the very early stage, see Fig. 1. In order to accelerate the clustering kinetics, it seemed tempting to exclude vacancies from consideration, allowing He atoms to migrate with the diffusion coefficient equal to the product of the vacancy diffusion coefficient and concentration. Such 'direct' He migration was simulated and indeed qualitatively reproduced vacancy-assisted He annealing kinetics, Fig. 1. However, the increased calculation efficiency allowed us to trace the He precipitation kinetics much further than in the exact vacancy-assisted simulation.

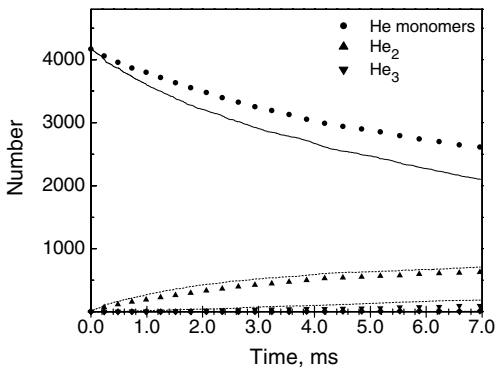


Fig. 1. Comparison of LKMC annealing of He atoms for vacancy-assisted (lines) and direct (points) He diffusion. Vacancy concentration is 100 ppm, He concentration – 1000 appm.

The discovered annealing kinetics turned out to be very far from what one might expected from the classical nucleation theory for a system consisting of one kind of mobile monomers. First of all, in spite of practically negligible thermal dissociation of He complexes (at the employed simulation temperature $T = 573$ K), clustering does not terminate with the expiration of He monomers, see Fig. 2(a), The reason is a pronounced mobility of small He clusters. Notably, He trimers annealed much faster than pairs, even though no special corrections for the He jump barrier reduction were introduced. This non-evident feature is purely topological and related to the fact that the movement of dimers on a bcc lattice requires an energy consumptive intermediate separation of the pair constituents from 1NN to 2NN distance, which is not necessary for a trimer (a detailed mechanism is discussed in [6] for the case of a tri-vacancy). After the trimers are fully annealed, the cluster ensemble kinetics is governed by the annealing of He pairs, Fig. 2(b). By the end of pair annealing, many very small (mostly 4–7 He atoms) clusters are formed.

### 3.2. Parallel He–He and V–V interaction

Switching on the V–V interaction in parallel with He–He binding leads to a picture completely different from that discussed in Section 3.1. The annealing kinetics is dominated by vacancy agglomeration into voids, which takes approximately one

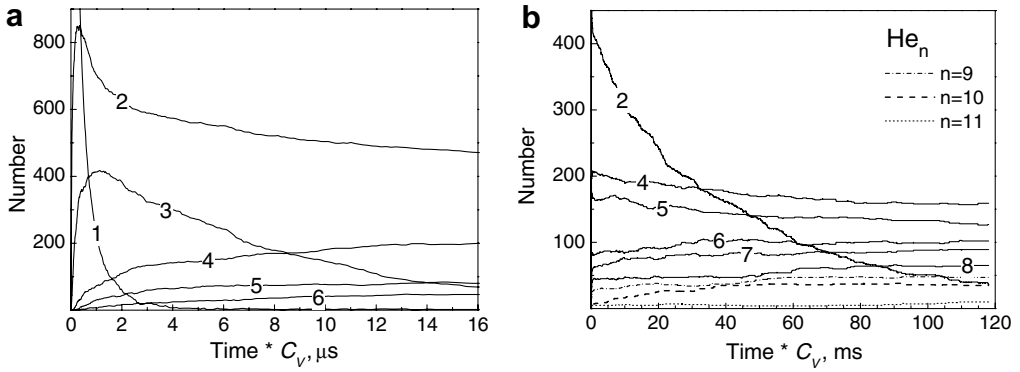


Fig. 2. Short-term (a) and long-term (b) kinetics of He annealing by direct diffusion. Numbers on the curves indicate the number of He atoms in cluster.

second. After that the system evolution can proceed only at the expense of vacancy thermal emission from voids, which occurs on longer time scales. The annealing of vacancies was practically insensitive to the presence of helium in the matrix. A comparison of two simulation runs, one with 1000 appm He and another without He, indicates that in both cases by the time when single vacancies are annealed out the void sizes are rather big and fall in the same range (10–30 vacancies per void), Fig. 3. The effect of vacancies on He clustering is weak, being mostly restricted to conversion of ~5% of He monomers into immobile helium pairs, Fig. 3(a).

### 3.3. Complete account of He–V interaction

Several simulations at different initial He concentrations (from 10 to 1000 appm) have been performed while accounting for all components of He and vacancy binding. Typical simulation run lengths were on the order of several hundred millions MCSs (corresponding to tens of milliseconds of annealing time at 573 K). In contrast to the case without He–V interaction, where little He clustering happened in such times, very pronounced annealing kinetics were observed, though the outcome of simulations depended very much on the initial He/V ratio. In particular, at $He/V \ll 1$ the dominant trend was vacancy clustering, the only difference from the free vacancy clustering being that some of the voids contained several (mostly 1–2) He atoms.

Quite different kinetics were observed in cases where the He concentration was the same or noticeably higher than that of vacancies. The dominant trend at the early stage (tenths of a microsecond) was the annealing of single vacancies and the formation of dimers $HeV_2$ (cluster size is determined in this paper by the number of vacancies in the cluster), followed by clusters of bigger sizes. The small He–V clusters demonstrated noticeable mobility and, after annihilation of single vacancies, the subsequent clustering kinetics were dominated by coalescence of small clusters. In the case of $He/V \sim 1$ we observed the consecutive peaks of the dimer and the trimer concentrations, Fig. 4(a). At a longer time scale (not shown in Fig. 4(a)), the concentrations of $He_nV_4$ complexes also tended to decrease, while the number density of clusters with bigger sizes progressively grew. Typically, the bigger the clusters, the later they appeared and the lower was their number density at a given annealing time, see insert in Fig. 4(a). The only exception to this trend was shown by the clusters $He_nV_{10}$. The He/V ratio in clusters varied, but on the average was close to $n/m \sim 0.5$. A certain amount of He (approximately a quarter) remained in solid solution, which indicated that the initial vacancy concentration should be somewhat bigger than that of He in order to trap all dissolved He atoms in bubbles.

Where the initial He/V ratio in a simulation cell was an order of magnitude higher than unity, vacancies were first captured by single He atoms and these complexes subsequently captured two more He atoms and within a microsecond the cluster population was dominated by $He_3V_4$ complexes, Fig. 4(b). A small concentration of bigger clusters was also formed quite early due to coalescence of

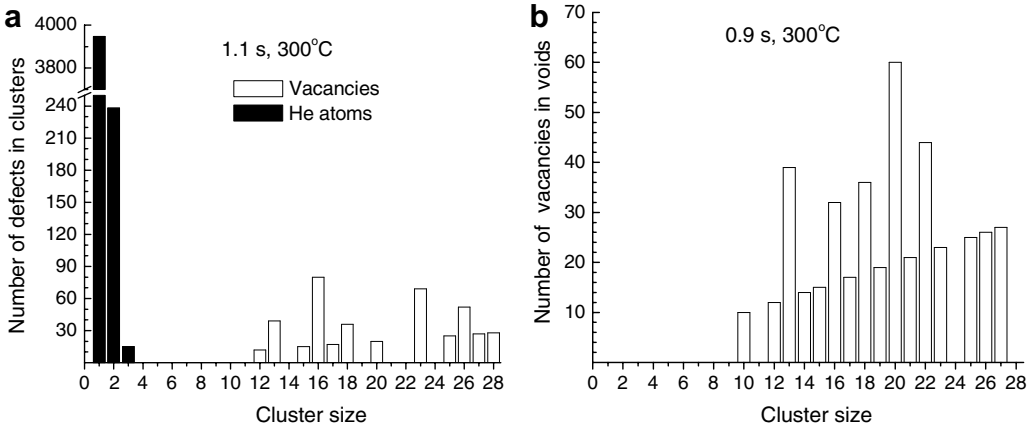


Fig. 3. Comparison of distribution of 100 ppm vacancies over clusters of different size after annealing for 40 millions MCSs in the absence of V–He binding. (a) 1000 appm He, (b) He-free cell.

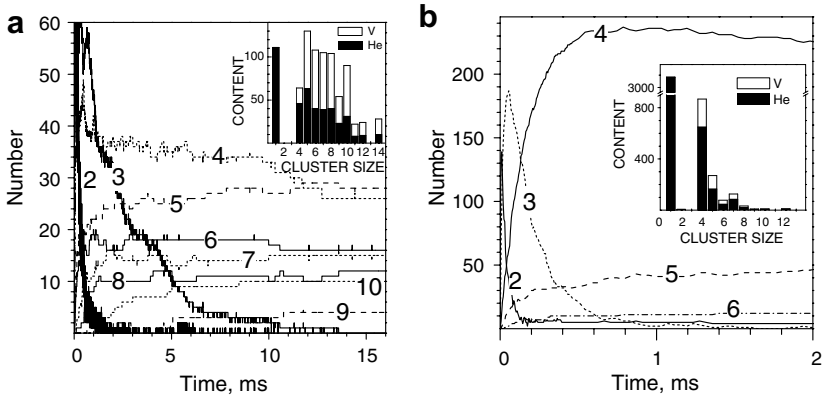


Fig. 4. Annealing kinetics of initially uniform solid solutions of 100 ppm vacancies with either 100 (a) or 1000 (b) appm He. Numbers on the curves indicate the number of vacancies, $m$, in clusters $He_nV_m$ (for all $n$). Inserts show the distributions of He atoms and vacancies over clusters of different sizes after LKMC annealing at 300 °C for ~80 ms (a) and ~8.5 ms (b).

very mobile $HeV_2$ and $He_2V_3$. After these mobile clusters had been annealed, the clustering noticeably slowed down, being governed by the annealing of poorly mobile $He_3V_4$.

### 3.4. Diffusivity of small He–V complexes

An interesting feature of the current simulation is the high mobility of small $He_nV_m$ complexes ($m > n$). Especially mobile are $HeV_2$ and $He_nV_3$, but the movements of bigger clusters could also be noticed by direct visualization. In order to get a feeling for relative complex mobility, the diffusion coefficients for several small He–V complexes at 573 K were estimated by LKMC. A detailed quantitative analysis of the small He–V cluster mobility and thermal stability is beyond the scope of this paper and will be reported elsewhere [13]. Here we would only like to emphasize that the noticeable mobility of small clusters is a topological feature and is retained even when one discards the vacancy–vacancy interaction induced reduction of the vacancy jump barrier, as described in Section 2, though the latter effect, naturally, does enhance the cluster mobility. A very similar effect of enhanced small cluster mobility was observed in MC simulations of copper annealing [14].

## 4. Conclusions

Our simulations indicate that in the absence of V–V and V–He binding the vacancy-assisted diffusion of helium can be reasonably approximated by direct helium migration. In the latter case the coalescence of mobile $He_2$ and $He_3$ complexes was found to play important part in He clustering kinetics.

The binding between vacancies and He atoms strongly influences He precipitation, involving very fast formation of small He–V clusters, which at 300 °C are sufficiently stable and mobile to provide a noticeable contribution to He clustering kinetics via cluster coalescence. The consequences of small He–V cluster mobility are especially pronounced where He concentration is comparable to or exceeds that of vacancies.

## Acknowledgements

One of the authors (V.B.) is grateful to FZ Karlsruhe for the funding of his research stay in FZK in the framework of the Guest Scientist program, The work was supported in part by grant No. 05-02-16994 from Russian Foundation for Basic Research.

## References

[1] X. Jia, Y. Dai, J. Nucl. Mater. 318 (2003) 207.
[2] J. Henry, M.H. Mathon, P. Jung, J. Nucl. Mater. 318 (2003) 249.
[3] C. Domain, C.S. Becquart, L. Malerba, J. Nucl. Mater. 335 (2004) 121.
[4] C.-C. Fu, F. Willaime, Phys. Rev. B 72 (2005) 064117.
[5] C. Domain, C.S. Becquart, Phys. Rev. B 65 (2001) 024103.
[6] C.-C. Fu, J.D. Torre, F. Willaime, J.L. Bocquet, A. Barbu, Nature Mater. 4 (1) (2005) 68.
[7] C. Becquart, C. Domain, Nucl. Instrum. and Meth. B 202 (2003) 44.
[8] T. Seletskaia, Yu. Osetsky, R.E. Stoller, G.M. Stocks, Phys. Rev. Lett. 94 (2005) 046403.

[9] K. Morishita, R. Sugano, B.D. Wirth, J. Nucl. Mater. 323 (2004) 243.
[10] B.D. Wirth, G.R. Odette, J. Marian, L. Ventelon, J.A. Young-Vandersall, L.A. Zepeda-Ruiz, J. Nucl. Mater. 329 (2004) 103.
[11] L.C. Kimerling, H.M. DeAngelis, J.W. Diebald, Solid State Commun. 16 (1975) 171.
[12] M.E.J. Newman, G.T. Barkema, Monte Carlo Methods in Statistical Physics, Clarendon, Oxford, 1999.
[13] V.A. Borodin, P.V. Vladimirov, J. Nucl. Mater., in press, doi:10.1016/j.jnucmat.2007.01.019.
[14] C. Domain, C.S. Becquart, J.C. van Duysen, Mater. Res. Soc. Symp. Proc. 540 (1999) 643.